Micromechanical Homogenisation of Steel Bars in Reinforced Concrete for Damage Analysis

Anastasios Drougkas (A.Drougkas@leeds.ac.uk), Vasilis Sarhosis

School of Civil Engineering, University of Leeds, Woodhouse Lane, LS2 9JT, Leeds, United Kingdom

Georgia Thermou

Department of Civil Engineering, The University of Nottingham, NG7 2RD Nottingham, United Kingdom

Abstract

A homogenisation scheme based on inclusion modelling is coupled with constitutive laws for damage and implemented in a finite element model for the simulation of concrete and reinforcement bar damage in reinforced concrete structures. The scheme is employed for simulating the behaviour of evenly distributed reinforcement and adapted for the simulation of zones with concentrated reinforcement in structural members.

The model is validated against experimental tests from the literature carried out on reinforced concrete members subjected to bending and direct tension. The model captures the main characteristics of the behaviour of and damage in the constituent materials of reinforced concrete without resorting to individual meshing of the embedded bars and with very low computational cost.

Keywords

- reinforced concrete
- micromechanics
- homogenisation
- damage modelling
- finite element analysis

Highlights

- A homogenisation scheme is applied in RC for simulating reinforced zones and surfaces

- Both distributed and concentrated reinforcement is simulated in full scale members
- Stresses, strains and damage in rebars and concrete can be calculated in a continuum FE mesh

1 Introduction

Modelling the damage initiation and propagation in reinforced concrete structures is critical for predicting their behaviour against a variety of actions. Cracks caused by mechanical loading, exposing the reinforcement bars to environmental effects and chemical attack, can significantly reduce durability and service life (Shaikh 2018). Additionally, excessive loading scenarios leading to cracking of the concrete can lead to a reduction of residual stiffness and strength in reinforced concrete members against future high demands, such as those arising during earthquake events (Shiradhonkar and Sinha 2018).

Reinforced concrete can be treated as a composite material consisting of two readily distinguishable phases with vastly different mechanical properties, behaviour and geometrical arrangement: the quasi-brittle concrete matrix and the ductile steel reinforcement. In a finite element analysis context, both material phases can be constitutively modelled and geometrically meshed individually (El-Gendy and El-Salakawy 2021; Markou and Roeloffze 2021; Moharrami and Koutromanos 2017). While adopting this approach for nonlinear analysis can produce comprehensive results on the stresses, strains and damage of the individual components of reinforced concrete, it can be demanding in terms of generating the geometry of the model as well as in computational terms for executing the calculations and processing the results (Markou and Genco 2019), especially when it becomes necessary to employ very fine finite element meshes for stable and accurate analysis (Cotsovos, Zeris, and Abas 2009). Reduction of computational cost can be achieved through adopting a plane stress approach. However, this approach means that the embedded bars need to be either simulated as embedded truss elements or as continuum elements interrupting the continuity of the concrete matrix. Both these approaches, therefore, introduce errors in the volume ratio and overall geometrical disposition of the matrix near the location of the bars.

Models for reinforced concrete members based on beam formulations, coupled with appropriate nonlinear constitutive laws, can substantially mitigate computational cost issues in finite element analysis (Lu et al. 2013; Santafé Iribarren et al. 2011). However, beam-based models are often unable to successfully capture all aspects of material nonlinearity in the components, especially in the rebars, due to inability of fully capturing the interaction of stress and strain between material phases in the composite.

Micromechanical homogenisation methods, as developed for composite materials consisting of inclusions embedded in a matrix (Eshelby 1957), can be employed for nonlinear analysis of reinforced concrete structures as an alternative to a pure finite element micromodel. These methods account for the full interaction of the phases in the composite and can often be expressed in closed form. While readily applicable for analysing the microstructure of plain concrete, namely modelling the interaction of hardened cement, aggregates, pores and cracks within the concrete (Nguyen, Stroeven, and Sluys 2012; Nilenius et al. 2014; Unger and Eckardt 2011; Wriggers and Moftah 2006; Wu and Wriggers 2015), homogenisation of the reinforced concrete itself has not received the same amount of attention. Specifically, while nonlinear analyses of reinforced concrete representative volume elements and structures with evenly distributed reinforcement have been performed (Combescure, Dumontet, and Voldoire 2015; Sciegaj et al. 2019; Teng et al. 2004), the simulation of reinforcement zones with concentrated reinforcement bars is not equally advanced within the context of micromechanical homogenisation. The presence of structural elements in building structures with clearly distinguishable reinforced zones, such as beams, limits the applicability of these homogenisation schemes in their present form.

In this paper a micromechanical homogenisation scheme based on the equivalent inclusion method is combined with nonlinear constitutive laws for concrete and reinforcement bar damage for simulating reinforced concrete elements under mechanical loading. A method for modelling reinforced zones is proposed and tested, in contrast to the typical micromechanical approach of assuming evenly distributed reinforcement. The homogenisation scheme and constitutive laws are subsequently implemented in a plane stress finite element model. The method is validated against experimental data from the literature involving full structural elements. The purpose of the proposed approach is to fully account for the interaction of the concrete with the embedded bars while maintaining computational complexity and costs low.

The paper sets off with the presentation of the homogenisation scheme for reinforcement bars embedded in concrete, with comments on the applicability of the scheme in reinforced concrete. Next, the constitutive laws for the damage models employed for the concrete and the bars are presented, along with the way these laws are incorporated in the overall modelling method. Next, the implementation of the scheme in a finite element context is described, along with a presentation of the modelling method adopted for reinforced zones. The verification of the model against experimental data involving reinforced concrete beams in bending and pure tension is subsequently presented, accompanied by general comments on the results produced by the model. Finally, the conclusions of this work are summarised and comments on future work are provided.

2 Micromechanical model

Reinforced concrete is treated as a composite material composed of a concrete matrix with orthogonally oriented embedded steel rebar inclusions (e.g., in case of a beam; flexural reinforcement: longitudinal bars, shear reinforcement: vertical or inclined bars), with their length being much larger than their cross-sectional dimensions. In the context of the modelling approach adopted, an isolated inclusion embedded in an infinitely large matrix undergoes deformation when the matrix itself is subjected to an average strain $\boldsymbol{\varepsilon}$ as a result of mechanical loading. In the general case where the matrix and inclusion have different elastic properties, the deformation of the inclusion is different from the average deformation of the matrix which constrains it. Removal of this constrain results in a strain state in the inclusion known as eigenstrain $\boldsymbol{\varepsilon}^*$. The relation between the strain of the matrix and of the inclusion is expressed as:

$$\varepsilon_{ij} = S_{ijkl}\varepsilon^*{}_{kl} \tag{1}$$

where S_{ijkl} are the components of Eshelby's fourth order tensor $\boldsymbol{S}$ (Eshelby 1957). Initial work on inclusion modelling was performed on ellipsoidal inclusions embedded in a three-dimensional matrix (Zou et al. 2010). The values in Eshelby's tensor are dependent on the dimension ratios of the ellipsoids. In the xy plane the ellipsoid reduces to an ellipse, the boundary of which is defined by the equation:

$$\frac{x^2}{{a_1}^2} + \frac{y^2}{{a_2}^2} = 1 \quad (2)$$

where a_1 and a_2 are the half-length and half-height of the ellipse in x and y respectively. Closed form expressions for Eshelby's tensor have been derived for elliptic inclusions in plane stress, the second order tensor being simply defined as (Huang, Zou, and Zheng 2009):

$$\boldsymbol{S} = \begin{bmatrix} S_{11} & S_{12} & 0 \\ S_{21} & S_{22} & 0 \\ 0 & 0 & S_{33} \end{bmatrix} \quad (3)$$

where:

$$\begin{aligned} S_{11} &= \frac{1}{k}(-3\varphi - 2 + 2\nu\varphi + 2\nu) \\ S_{22} &= \frac{1}{k}\varphi(-2\varphi - 3 + 2\nu\varphi + 2\nu) \\ S_{12} &= -\frac{1}{k}(-\varphi + 2\nu\varphi + 2\nu) \\ S_{21} &= -\frac{1}{k}\varphi(-1 + 2\nu\varphi + 2\nu) \\ S_{33} &= \frac{1}{k}(\varphi + (\nu - 1)(1 + \varphi)^2) \end{aligned} \quad (4)$$

with:

$$\begin{aligned} k &= 2(\nu - 1)(1 + \varphi)^2 \\ \varphi &= \frac{a_1}{a_2} \end{aligned} \quad (5)$$

Plane stress conditions are deemed adequate for a wide variety of applications where the transversal dimension of the simulated structural elements is small or when the confinement of the concrete is not of primary importance.

Needle-shaped, or cylindrical, inclusions oriented along the x axis are derived from elliptical inclusions with dimension a_1 being much greater than a_2, to the effect that in the present context $\varphi \to +\infty$. Based on this assumption, the values of Eshelby's tensor for needle inclusions oriented along the x in plane stress are as follows:

$$\boldsymbol{S} = \begin{bmatrix} 0 & 0 & 0 \\ \dfrac{\nu_m}{1-\nu_m} & 1 & 0 \\ 0 & 0 & 0.5 \end{bmatrix} \tag{6}$$

where ν_m is the Poisson's ratio of the matrix m. The $\boldsymbol{S}$ tensor for needle inclusions oriented along the y axis can be simply produced by substitution between the 1 and 2 indices in eq. (4) while the 3 indices corresponding to the shear component of the eigenstrain remain unaltered. A conceptual illustration of a composite material C in xy two-dimensional space with two networks of evenly spaced needle inclusions i_x and i_y oriented along the x and y axes within a matrix m is shown in Figure 1.

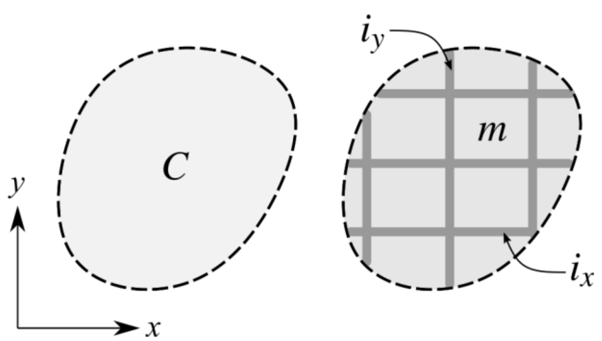

Figure 1 **Composite material $\boldsymbol{C}$ composed of needle inclusions $\boldsymbol{i_x}$ and $\boldsymbol{i_y}$ embedded in matrix $\boldsymbol{m}$.**

Inclusions with identical properties, shape and orientation in a composite material can be considered in groups. Under the dilute approximation for inclusions, the dilute estimate $\boldsymbol{T}_i$ of the i-th group of inclusions is equal to:

$$\boldsymbol{T}_i = \left(\boldsymbol{I} + \boldsymbol{S}_i(\boldsymbol{C}_m)^{-1}(\boldsymbol{C}_i - \boldsymbol{C}_m)\right)^{-1} \tag{7}$$

where $\boldsymbol{I}$ is the 3×3 identity tensor and $\boldsymbol{C}_m$ and $\boldsymbol{C}_i$ are the plane stress stiffness tensors of the matrix and the inclusion respectively, functions of the Young's moduli and Poisson's ratios of the individual materials.

The matrix strain concentration factor $\boldsymbol{A}_C$ is a function of the dilute estimates of all inclusion groups present in the composite and is equal to:

$$\boldsymbol{A}_C = \left(\omega_m \boldsymbol{I} + \sum_{i=1}^{n} \omega_i \boldsymbol{T}_i \right)^{-1} \tag{8}$$

where ω_i is the volume ratio of the i-th group of inclusions, ω_m the volume ratio of the matrix with respect to the total volume of the composite and n is the total number of inclusion groups. The sum of all volume ratios is equal to 1. The strain concentration tensor $\boldsymbol{A}_i$ of the i-th inclusion group within the composite material is equal to:

$$\boldsymbol{A}_i = \boldsymbol{T}_i \boldsymbol{A}_C \tag{9}$$

Finally, the effective stiffness tensor $\boldsymbol{C}_C$ of the composite material can be calculated in closed form according to the equation (Marzari and Ferrari 1992):

$$\boldsymbol{C}_C = \boldsymbol{C}_m + \sum_{i=1}^{n} \omega_i (\boldsymbol{C}_i - \boldsymbol{C}_m) \boldsymbol{A}_i \tag{10}$$

Having calculated the effect of the inclusions on the matrix, the stresses and strains in all components of the composite material can be calculated, which is essential for damage analysis. As such, the strain vector in the matrix $\boldsymbol{\varepsilon}_m$ is equal to (Mori and Tanaka 1973):

$$\boldsymbol{\varepsilon}_m = \boldsymbol{A}_C \boldsymbol{\varepsilon}_C \tag{11}$$

where $\boldsymbol{\varepsilon}_C$ is the macroscopic strain vector in the composite. The stress vector $\boldsymbol{\sigma}_m$ in the matrix is equal to:

$$\boldsymbol{\sigma}_m = \boldsymbol{C}_m \boldsymbol{\varepsilon}_m \tag{12}$$

The strain vector $\boldsymbol{\varepsilon}_i$ in the i-th group of inclusions is equal to (Benveniste 1987):

$$\boldsymbol{\varepsilon}_i = \boldsymbol{A}_i \boldsymbol{\varepsilon}_c \tag{13}$$

and the stress vector $\boldsymbol{\sigma}_i$ is equal to:

$$\boldsymbol{\sigma}_i = \boldsymbol{C}_i \boldsymbol{A}_i (\boldsymbol{C}_C)^{-1} \boldsymbol{\sigma}_C \tag{14}$$

where $\boldsymbol{\sigma}_C$ is the macroscopic stress vector in the composite, equal to:

$$\boldsymbol{\sigma}_C = \boldsymbol{C}_C \boldsymbol{\varepsilon}_C \tag{15}$$

In the present work, the concrete serves as the matrix in which the embedded reinforcement bars serve as the inclusions in two groups. The typically large ratio of the length of the bars over their diameter lends itself to the assumption of their being needle-shaped in this context. Further, the typical orthogonal orientation of the bars with respect to the orientation of cuboid shaped reinforced concrete elements, such as slabs, beams, columns and walls, allows the homogenisation calculations to be performed without complex consideration of the orientation of the inclusions. This fact, coupled with the assumption of needle shaped inclusions, allows the expression of the entire homogenisation scheme in closed form, thus further reducing computational complexity. Application of the same homogenisation scheme in three dimensions is identical to the presented process, with only Eshelby's tensor $\boldsymbol{S}$ assuming different size and values (Qiu and Weng 1990) and the stiffness tensors for three dimensional elasticity needing to be adopted. In such an approach a third inclusion group, oriented in the z axis, can also be included while maintaining the closed form of the scheme.

3 Constitutive modelling

Concrete can fail in compression and tension, while reinforcement bars can yield in compression or tension. Loss of stiffness in the components of the composite material is calculated in a damage mechanics approach (Kachanov 1958; Voyiadjis and Kattan 2017). In this context, the stiffness tensors of the components are multiplied with integrity variables, which start off from 1 for an undamaged material and tend towards zero for a completely softened material. These integrity variables express the ratio between the actual damaged stress and the effective stress, which is proportional to the strain. Damage in these components results in a loss of stiffness of the composite material as calculated according to eqs. (7) to (10).

Failure of concrete in compression is modelled through a stress strain curve consisting of an initial linear part followed by a parabolic hardening-softening curve (Feenstra and De Borst 1996)based on compressive fracture energy. As such, the integrity variable of the concrete matrix in compression I_c as a function of the strain ε is equal to:

$$I_c(\varepsilon) = \begin{cases} 1 & \varepsilon_l \le \varepsilon \le 0 \\ -\dfrac{f_c}{\sigma_e}\dfrac{1}{3}\left(1 + 4\dfrac{\varepsilon - \varepsilon_c^l}{\varepsilon_c^p - \varepsilon_c^l} - 2\left(\dfrac{\varepsilon - \varepsilon_c^l}{\varepsilon_c^p - \varepsilon_c^l}\right)^2\right) & \varepsilon_c^p \le \varepsilon \le \varepsilon_c^l \\ -\dfrac{f_c}{\sigma_e}\left(1 - \left(\dfrac{\varepsilon - \varepsilon_c^p}{\varepsilon_c^u - \varepsilon_c^p}\right)^2\right) & \varepsilon_c^u \le \varepsilon \le \varepsilon_c^p \\ 0 & \varepsilon \le \varepsilon_c^u \end{cases} \tag{16}$$

where f_c is the compressive strength of the component (negative value), σ_e is the effective stress and ε_c^l, ε_c^p and ε_c^u being the limit of proportionality, peak strain and ultimate strain in compression respectively, equal to:

$$\begin{gathered} \varepsilon_c^l = \frac{f_c}{3E_c} \\ \varepsilon_c^p = 5\varepsilon_l \\ \varepsilon_c^u = \frac{G_c}{f_c h} \end{gathered} \tag{17}$$

where E_c is the Young's modulus of the concrete, G_c is its compressive fracture energy and h is the bandwidth, meaning the length at which the constitutive law is being evaluated.

Cracking damage in concrete due to tension is modelled through linear behaviour up to peak stress and an exponential softening curve thereafter based on tensile fracture energy. The integrity variable for tension I_t is equal to:

$$I_t\,(\varepsilon) = \begin{cases} 1 & 0 \le \varepsilon \le \varepsilon_t^p \\ \dfrac{f_t}{\sigma_e}\exp\left(-\dfrac{\varepsilon - \varepsilon_t^p}{\varepsilon_t^u}\right) & \varepsilon_t^p \le \varepsilon \end{cases} \tag{18}$$

where f_t is the tensile strength and ε_t^p and ε_t^u being the peak strain and ultimate strain in tension respectively. These are equal to:

$$\varepsilon_t^p = \frac{f_t}{E_c}$$
$$\varepsilon_t^u = \frac{G_t}{f_t h} \tag{19}$$

where G_t is the tensile fracture energy.

Yielding of the reinforcement in tension or compression is considered through an elastic and perfectly plastic response. The integrity variable I_y can be thus expressed as:

$$I_y(\varepsilon) = \begin{cases} 1 & 0 \leq \varepsilon \leq \varepsilon_y \\ \dfrac{f_y}{|\sigma_e|} & \varepsilon_y \leq \varepsilon \end{cases} \tag{20}$$

where f_y is the yielding strength of the reinforcement and ε_y is the yielding strain, equal to:

$$\varepsilon_y = \frac{f_y}{E_s} \tag{21}$$

where E_s is the Young's modulus of the reinforcement.

These constitutive equations for concrete and reinforcement damage allow for the most typical failure modes observed in reinforced concrete members to be simulated. In this investigation bond-slip between the concrete and reinforcement is not considered since the homogenisation scheme in its present implementation assumes perfect bond between the bars and the concrete. However, bond-slip can be implemented in the same modelling context in future work. The implemented constitutive laws are illustrated in the stress-strain diagrams of Figure 2.

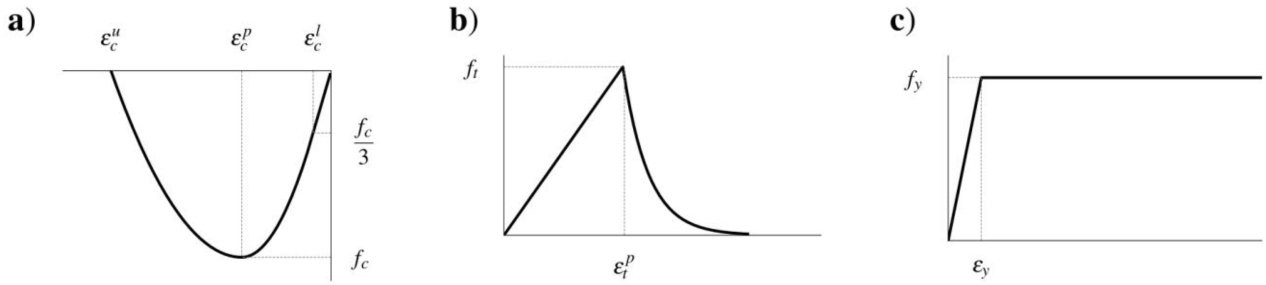

Figure 2 Stress-strain constitutive laws for damage in components: a) concrete in compression, b) concrete in tension, c) reinforcement in axial tension/compression.

4 Finite element implementation

The homogenisation scheme and constitutive stress-strain laws have been implemented in the FEniCS finite element platform (Alnæs et al. 2015) in plane stress conditions. The homogenisation approach employed allows for simulating the contribution of the reinforcement bars to the stiffness and strength of the reinforced concrete without the need to individually mesh the embedded bars, thus substantially reducing modelling complexity. For finite element analysis the homogenisation process is implemented differently for longitudinal (flexural) and transversal (shear) reinforcement, which are treated as different inclusion groups.

Longitudinal bars in reinforced concrete beams are often concentrated in reinforced zones near the lower and upper regions of the cross section. Similar arrangements are often encountered in columns. Therefore, the volume ratio for the longitudinal bars was calculated according to the local amount of reinforcement in each reinforced zone. Outside of the reinforced zone the volume ratio of the longitudinal reinforcement is zero. This approach allows the correct assignment of volume ratios for reinforcement and concrete throughout the section, and for modelling the full stress and strain interaction of the components, while remaining in plane stress conditions. An illustration of the concept of the reinforced zone is illustrated in Figure 3.

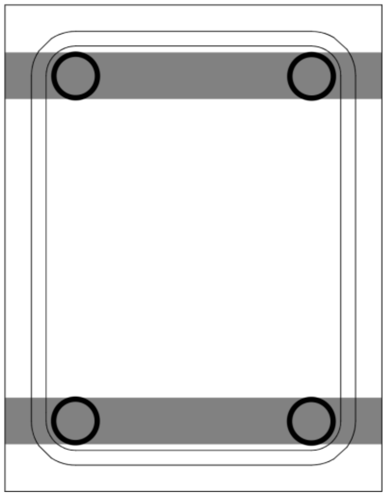

Figure 3 Cross section of reinforced concrete beam. Reinforced zones containing longitudinal bars shaded.

Transversal reinforcement is distributed along the length of the beam in regions with constant spacing. Therefore, a constant volume ratio can be applied in each region to take the effect of the transversal reinforcement into account, as is typical in micromechanical homogenisation of composites with evenly distributed oriented inclusions. Alternatively, the volume ratio of transversal reinforcement can be introduced in the model through simple spatial functions, allowing the modelling of structural elements with arbitrarily variable reinforcement spacing.

Evaluation of the compressive integrity is done against the minimum principal strain while the tensile integrity is evaluated against the maximum principal strain in the concrete matrix, calculated from eq. (11). Yielding in the reinforcement is evaluated along the orientation axis of the inclusion, thus accounting for axial yielding of the bars in tension or compression.

An isotropic damage approach is adopted in this study. Consequently, the stiffness tensor of the concrete is multiplied with the integrity variables in compression and tension while the reinforcement stiffness tensor is multiplied with the yielding integrity variable. As a result, damage in one direction results in loss of stiffness in all directions for the evaluated material component. Additionally, damage is considered irreversible. Thus, reduction in strain between load steps in a component does not lead to potential increase of the integrity. The approach of adopting integrity variables at the micro level of the individual components means that loss of stiffness in the reinforced concrete is not directly expressed at the macro level of the composite material with a single variable.

The bandwidth h for the softening curves in eq. (16) and (18) (20)is taken as equal to the characteristic finite element length at the location of evaluation, namely the square root of the surface area of the element where the curves are evaluated. Nonlinear analysis is performed through the use of a Newton-Raphson method in force control.

5 Model validation

5.1 Reinforced concrete beams in bending

The proposed model is firstly validated against two experimental tests performed on reinforced concrete beams in three-point bending (Qin, Zhou, and Lau 2017). The beams were simply supported and loaded with a single concentrated vertical force applied at mid span. An illustration of the overall layout of these beams is shown in Figure 4. The longitudinal reinforcement was constant in the tensile and compression zones. The spacing of the transversal reinforcement was constant in the span and reduced near the supports. The beams have been characterised as “under-reinforced” by the authors of the cited work, owing to the low amount of longitudinal reinforcement with respect to the total cross-sectional dimensions of the specimens. The low reinforcement ratio induces substantial strain on the longitudinal bars when the beams are subjected to bending. Therefore, these experiments are considered ideal for validating the proposed homogenisation scheme.

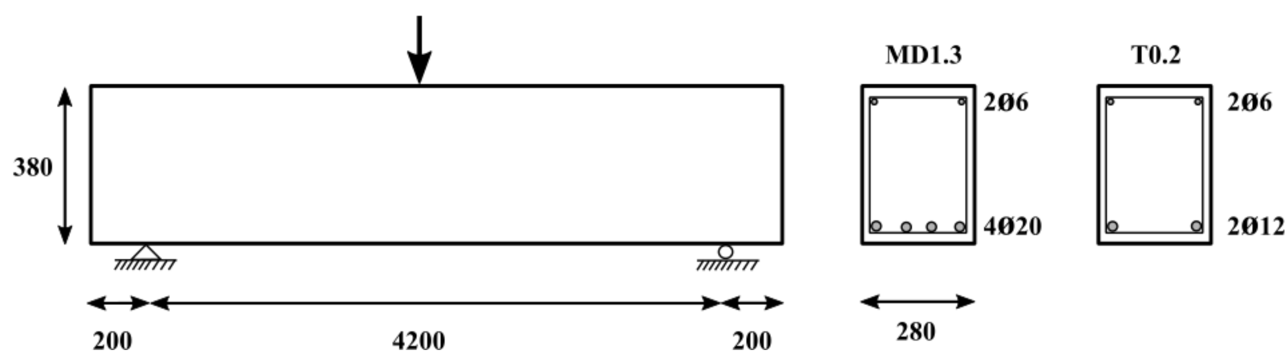

Figure 4 Geometric, loading and reinforcement layout of reinforced concrete beams MD1.3 and T0.2. Dimensions in mm.

The two specimens, designated MD1.3 and T0.2, had the same geometry, loading layout and transversal reinforcement, but different longitudinal reinforcement and mean material properties as shown in Table 1. Some material parameters necessary for nonlinear analysis based on the employed constitutive laws were missing from the reported properties. Values found in the relevant literature were used in their stead. Considering the reported value of the compressive strength f_c as the mean value, the tensile strength of concrete f_t was calculated as (CEN 2004):

$$f_t = 0.30(-f_c - 8)^{2/3} \tag{22}$$

Similarly, the Young's modulus of concrete E_c was calculated as (CEN 2004):

$$E_c = 22000\left(\frac{-f_c}{10}\right)^{0.3} \tag{23}$$

The density ρ of reinforced concrete was taken as equal to 2500 $\mathrm{kg/m^3}$. The Poisson's ratio of steel ν_s was taken as equal to 0.280. The tensile fracture energy of concrete G_t was calculated based on the Model Code 2010 equation (Federátion Internationale du Béton 2013):

$$G_t = 0.073(-f_c)^{0.18} \tag{24}$$

while the compressive fracture energy of concrete in compression G_c was calculated using the equation (Drougkas, Roca, and Molins 2015):

$$G_c = -f_c d \tag{25}$$

where d is a ductility index equal to 1 mm.

Table 1 Properties of MD1.3 and T0.2 reinforced concrete beam components. Assumed values in italics.

Component	Property	Symbol	Units	MD1.3	T0.2
Concrete	Young's modulus	E_c	N/mm^2	*33093*	*32118*
	Poisson's ratio	ν_c	–	0.167	0.167
	Density	ρ	kg/m^3	*2500*	*2500*
	Compressive strength	f_c	N/mm^2	-39.0	-35.3
	Tensile strength	f_t	N/mm^2	*2.96*	*2.72*
Steel	Young's modulus	E_s	N/mm^2	189000	220500
	Poisson's ratio	ν_s	–	*0.280*	*0.280*
	Yield strength	f_y	N/mm^2	341	507
	Tensile zone reinforcement	A_{s1}	mm^2	1256	226
	Compressive zone reinforcement	A_{s2}	mm^2	57	57
	Shear reinforcement	A_{sw}	mm^2	100	100
	Shear reinforcement spacing	s	mm	50 - 100	50 - 100

The finite element model for simulating the beam experiments consisted of a mesh of 1276 plane stress linear triangular elements. The properties within the lower and upper reinforced zones were assigned the appropriate volume ratios for the x oriented inclusions, as per the proposed reinforced zone concept. A single vertical axis of symmetry was employed at mid span for reduction of the model size.

The results of the experimental tests are compared with the nonlinear analysis results in terms of peak force and vertical displacement at mid span at failure in Table 2. The predicted values are in good agreement with the experimental results, particularly in the MD1.3 case. An overestimation was obtained in the predicted displacement at failure, more notable in the T0.2 case. This discrepancy was considered minor as it could potentially be due to a difference between the actual Young's modulus of concrete E_c and the values assumed in the analysis.

Table 2 Comparison of experimental with numerical results for beams in bending. Percentile difference in parentheses.

	Peak force		Failure displacement at mid span	
Case	**Experiment**	**Numerical**	**Experiment**	**Numerical**
MD1.3	140.38 kN	146,68 kN (+4,49%)	193.6 mm	181,3 mm (-6,35%)
T0.2	41.90 kN	44.80 kN (+6.92%)	86.0 mm	84,6 mm (-1,63%)

An illustration of the numerically obtained failure mode is shown in Figure 5. The MD1.3 case is used for illustrating the failure mode, with the T0.2 case producing similar results. The failure mode is presented in terms of the integrity variable of concrete in tension I_c, the loss of which can lead to the formation of visible tensile cracks. The development of the loss of integrity is shown for increasing applied load. Damage due to bending arises at the tensile zone at mid span. The damaged zone increases in length and height for an increase in the load until the peak force is obtained, at which point the damage has propagated nearly to the top of the cross section at mid span. This response is typical of simply supported beams and is in agreement with the behaviour obtained both in the experiments and in their numerical reproduction in the cited source (Qin et al. 2017).

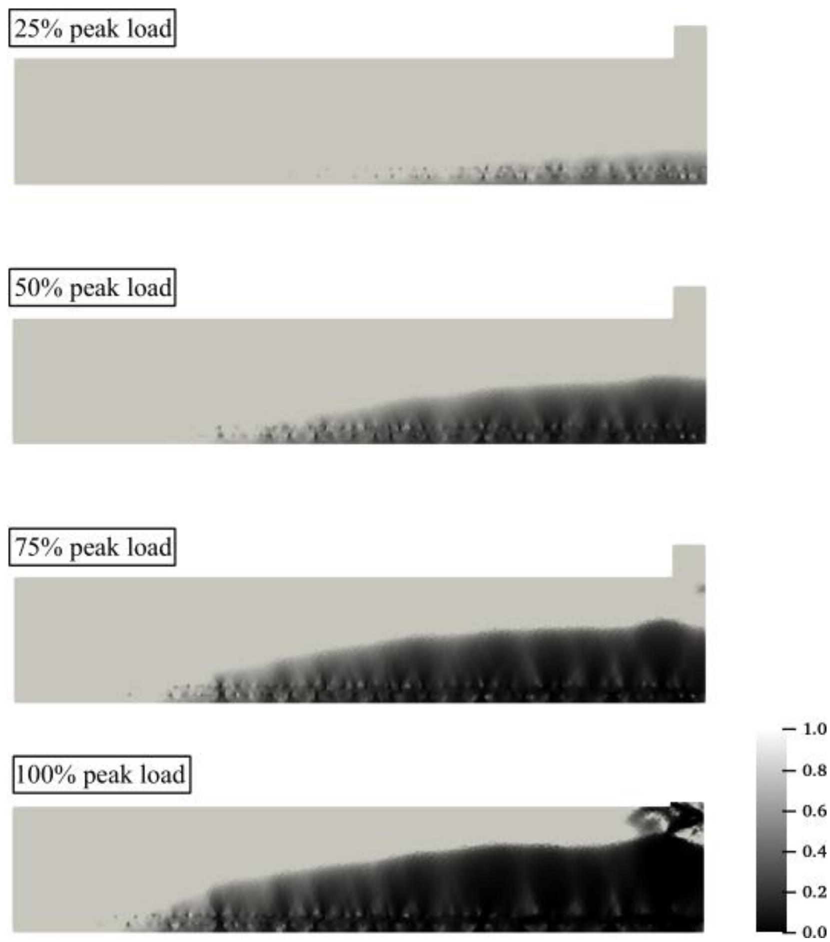

Figure 5 Numerically obtained failure mode for reinforced concrete beams. Integrity variable of concrete in tension I_t at 25%, 50% 75% and 100% peak load.

For demonstrating the capacity of the proposed model to produce discretised damage in a clearer fashion, the tensile crack patterns can be visualised by plotting maximum principal strains at 100% peak load, as can be seen in Figure 6 for case MD1.3. The average crack spacing for case MD1.3 is 73 mm while for case T0.2 it is equal to 66 mm.

Figure 6 Crack pattern of beam at 100% peak load in terms of maximum principal strain.

The behaviour of the longitudinal bars may also be readily evaluated through the model. The axial stresses of the longitudinal bars at peak force are shown in Figure 7. It can be observed that the distribution of axial stresses is typical of simply supported beams at failure: yielding of the lower bars in tension at mid span, with the magnitude of stresses decreasing farther away from that location. Similarly, the upper bars are yielding in compression at mid span.

Figure 7 Axial stresses ($\mathrm{N/m^2}$) in longitudinal bars at peak force.

The assumption of infinite aspect ratio does not hold for the transversal reinforcement bars. The actual aspect ratio of the transversal reinforcement is equal to 42.5, which is, nevertheless, high. The difference in the terms of Eshelby's tensor $\boldsymbol{S}$ between assuming an infinite aspect ratio and an aspect ratio equal to 42.5 is, at maximum, roughly 6%. The numerical results were found to not be sensitive to this difference. Therefore, the infinite aspect ratio assumption was maintained for this case.

Overall, the model validation demonstrates the viability of the reinforced zone concept for reinforced concrete elements with concentrated rather than evenly distributed bars. The plane stress assumption maintains computational cost very low, allowing for numerical experiments and parametric studies.

5.2 Reinforced concrete beams in tension

A second validation study of the proposed model is performed against two experimental cases of reinforced concrete beams subjected to direct tension (Ouyang et al. 1997). The beams, designated as NSC

3 × 9.5 and HSC 3 × 9.5, standing for normal strength and high strength concrete respectively, are reinforced with three longitudinal bars, evenly distributed along the height of the element. Two notches, each 10 mm deep and 12.7 mm wide, were provided at the centre of the beams for localising the formation of the first cracks in the concrete. The experimental cases are deemed ideal for validating the proposed homogenisation approach. The experiments are controlled to a large extent by the plastic behaviour of the longitudinal reinforcement. The overall layout of the beams, their loading scheme and their cross section are shown in Figure 8.

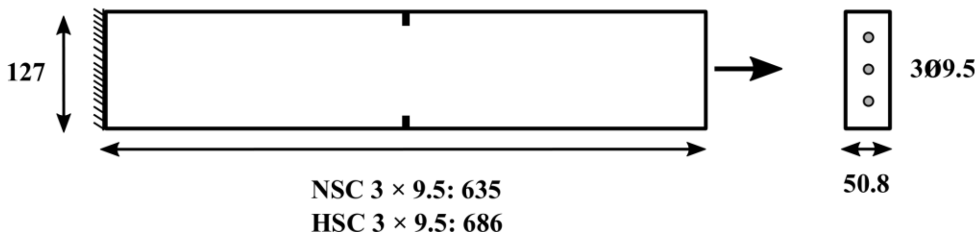

Figure 8 Geometric, loading and reinforcement layout of reinforced concrete beams NSC 3 × 9.5 and HSC 3 × 9.5. Dimensions in mm.

The material parameters used for numerical analysis are presented in Table 3. For this case only the Poisson's ratios of the components and the compressive fracture energy of the concrete (which does not play a substantial role in this test) needed to be assumed, as the remaining values were provided by the authors (Ouyang et al. 1997).

Table 3 Properties of NSC 3 × 9.5 and HSC 3 × 9.5 reinforced concrete beam components. Assumed values in italics.

Component	Property	Symbol	Units	NSC 3 × 9.5	HSC 3 × 9.5
Concrete	Young's modulus	E_c	N/mm^2	27349	36624
	Poisson's ratio	ν_c	–	*0.175*	*0.175*
	Density	ρ	kg/m^3	*2500*	*2500*
	Compressive strength	f_c	N/mm^2	-44.0	-99.1
	Tensile strength	f_t	N/mm^2	3.19	5.52
Steel	Young's modulus	E_s	N/mm^2	191584	191584
	Poisson's ratio	ν_s	–	*0.280*	*0.280*
	Yield strength	f_y	N/mm^2	508	508
	Axial reinforcement	A_s	mm^2	213	213

For this analysis the longitudinal reinforcement was considered evenly distributed across the height of the beam. Therefore, the concept of the reinforced zone was not employed, the longitudinal reinforcement ratio being considered constant throughout the area of the model. Transversal reinforcement was not included in the calculations. A coarse mesh of 416 linear triangular finite elements was employed for testing the capacity of the proposed model to perform accurately with low density meshes.

The results of the experimental test and the numerical results are presented in terms for force-displacement curves in Figure 9. The initial stiffness, the stiffness after cracking of the concrete (namely the stiffness provided to the composite by the bars), the displacement at failure and the peak force are very well approximated by the model. The loss of stiffness immediately after the initial elastic part of the response is not equally well captured by the model, possibly due to the lack of modelling of the bond slip, meaning that the stiffness of the perfectly bonded bars is immediately activated after cracking of the concrete. Additionally, the cracking load for the HSC 3 × 9.5 case is overestimated in the analysis, potentially due to a discrepancy between the average experimental value of the tensile strength of concrete and the in-situ strength in the specimen. Finally, the strain hardening phase in the HSC 3 × 9.5 case appears to last longer than in the experimental case, with the global structural stiffness reaching the experimentally obtained value near failure. This is potentially due to an overestimation of the tensile fracture energy.

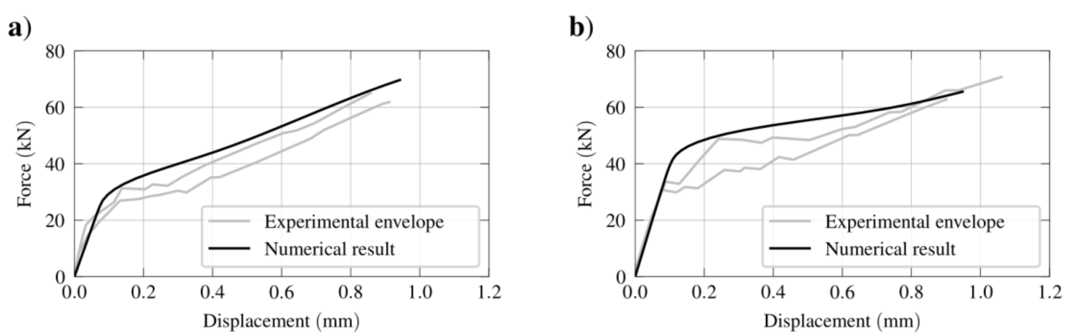

Figure 9 Comparison of experimental with numerical results for beams in tension: a) NSC 3 × 9.5 and b) HSC 3 × 9.5 specimens.

The accuracy of the model in simulating this experimental case demonstrates the suitability of the proposed approach in capturing the behaviour of reinforced concrete structures with evenly distributed bars without resorting to the reinforced zone approach. This approach is accurate and efficient with coarse finite element meshes, thus significantly reducing computational costs and modelling complexity for large structural elements.

6 Conclusions

A homogenisation scheme for reinforced concrete structures based on inclusion micromechanics, combined with constitutive modelling of material failure based on damage mechanics, is developed and implemented in a finite context for nonlinear analysis. The proposed scheme is able to capture the salient characteristics of the behaviour of concrete and reinforcement bars in reinforced concrete without resorting to distinct meshing of the reinforcement bars embedded in the concrete. The model is able to predict the capacity of reinforced concrete beams with good accuracy, low computational cost and low geometrical modelling effort.

The proposed scheme can account for both distributed reinforcement as well as for zones with concentrated reinforcement through a simple adjustment of material parameters assigned to specific regions of the finite element mesh. This allows for correct assignment of reinforcement and concrete volume ratios throughout the analysis domain and for complete simulation of stress and strain interaction between components of the composite while remaining within plane stress conditions.

One aspect of future work along this research path includes the simulation of bond-slip failure and dowel action of the bars. This can be accomplished through the introduction of the necessary longitudinal strain component in the bars and its evaluation against an appropriate constitutive model for slipping, while the latter can be achieved through evaluation of the shear stress and strain in the bars against a similarly appropriate constitutive law. Further constitutive modelling of confined concrete can be implemented for simulating the confinement effect provided by the reinforcement bars.

A further aspect of future work is the simulation of mechanically anchored repair and strengthening measures, such as reinforced concrete jackets, or externally bonded composites, such as textile reinforced composites and mortars, again employing the homogenisation scheme proposed here for the bars.

References

Alnæs, Martin S., Jan Blechta, Johan Hake, August Johansson, Benjamin Kehlet, Anders Logg, Chris Richardson, Johannes Ring, Marie E. Rognes, and Garth N. Wells. 2015. “The FEniCS Project Version 1.5.” *Archive of Numerical Software* 3(100).

Benveniste, Y. 1987. “A New Approach to the Application of Mori-Tanaka’s Theory in Composite Materials.” *Mechanics of Materials* 6(2):147–57.

CEN. 2004. *EN 1992-1-1 — Eurocode 2: Design of Concrete Structures - Part 1-1: General Rules and Rules for Buildings*.

Combescure, Christelle, Hélène Dumontet, and François Voldoire. 2015. “Dissipative Homogenised Reinforced Concrete (DHRC) Constitutive Model Dedicated to Reinforced Concrete Plates under Seismic Loading.” *International Journal of Solids and Structures* 73–74:78–98.

Cotsovos, Demetrios M., C. Zeris, and A. Abas. 2009. “Finite Element Modeling of Structural Concrete.” in *ECCOMAS thematic conference on computational methods in structural dynamics and earthquake engineering*.

Drougkas, Anastasios, Pere Roca, and Climent Molins. 2015. “Numerical Prediction of the Behavior, Strength and Elasticity of Masonry in Compression.” *Engineering Structures* 90:15–28.

El-Gendy, Mohammed G., and Ehab F. El-Salakawy. 2021. “Finite-Element Analysis of FRP-Reinforced Concrete Slab-–Column Edge Connections Subjected to Reversed-Cyclic Lateral Loads.” *Journal of Composites for Construction* 25(1):04020082.

Eshelby, J. D. 1957. “The Determination of the Elastic Field of an Ellipsoidal Inclusion, and Related Problems.” *Proceedings of the Royal Society of London. Series A, Mathematical and Physical Sciences* 241(1226):376–96.

Federátion Internationale du Béton. 2013. *The Fib Model Code for Concrete Structures 2010*. Wiley and Sons.

Feenstra, P. H., and René De Borst. 1996. “A Composite Plasticity Model for Concrete.” *International Journal of Solids and Structures* 33(5):707–30.

Huang, Mojia, Wennan Zou, and Quan Shui Zheng. 2009. “Explicit Expression of Eshelby Tensor for Arbitrary Weakly Non-Circular Inclusion in Two-Dimensional Elasticity.” *International Journal of Engineering Science* 47(11–12):1240–50.

Kachanov, L. M. 1958. “Time of the Rupture Process under Creep Conditions, Izy Akad.” *Nank S. S. R. Otd*

Tech Nauk 8:26–31.

Lu, Xiao, Xinzheng Lu, Hong Guan, and Lieping Ye. 2013. “Collapse Simulation of Reinforced Concrete High-Rise Building Induced by Extreme Earthquakes.” *Earthquake Engineering \& Structural Dynamics* 42(5):705–23.

Markou, George, and Filippo Genco. 2019. “Seismic Assessment of Small Modular Reactors: NuScale Case Study for the 8.8 Mw Earthquake in Chile.” *Nuclear Engineering and Design* 342:176–204.

Markou, George, and Wynand Roeloffze. 2021. “Finite Element Modelling of Plain and Reinforced Concrete Specimens with the Kotsovos and Pavlovic Material Model, Smeared Crack Approach and Fine Meshes.” *International Journal of Damage Mechanics* 30(6):845–71.

Marzari, Nicola, and Mauro Ferrari. 1992. “Textural and Micromorphological Effects on the Overall Elastic Response of Macroscopically Anisotropic Composites.” *Journal of Applied Mechanics* 59(2):269–75.

Moharrami, Mohammadreza, and Ioannis Koutromanos. 2017. “Finite Element Analysis of Damage and Failure of Reinforced Concrete Members under Earthquake Loading.” *Earthquake Engineering and Structural Dynamics* 46(15):2811–29.

Mori, T., and K. Tanaka. 1973. “Average Stress in Matrix and Average Elastic Energy of Materials with Misfitting Inclusions.” *Acta Metallurgica* 21(5):571–74.

Nguyen, Vinh Phu, Martijn Stroeven, and Lambertus Johannes Sluys. 2012. “Multiscale Failure Modeling of Concrete: Micromechanical Modeling, Discontinuous Homogenization and Parallel Computations.” *Computer Methods in Applied Mechanics and Engineering* 201–204:139–56.

Nilenius, Filip, Fredrik Larsson, Karin Lundgren, and Kenneth Runesson. 2014. “Computational Homogenization of Diffusion in Three-Phase Mesoscale Concrete.” *Computational Mechanics* 54(2):461–72.

Ouyang, C., E. Wollrab, S. M. Kulkarni, and S. P. Shah. 1997. “Prediction of Cracking Response of Reinforced Concrete Tensile Members.” *Journal of Structural Engineering* 123(1):70–78.

Qin, Renyuan, Ao Zhou, and Denvid Lau. 2017. “Effect of Reinforcement Ratio on the Flexural Performance of Hybrid FRP Reinforced Concrete Beams." *Composites Part B: Engineering* 108:200–209.

Qiu, Y. P., and G. J. Weng. 1990. "On the Application of Mori-Tanaka's Theory Involving Transversely Isotropic Spheroidal Inclusions." *International Journal of Engineering Science* 28(11):1121–37.

Santafé Iribarren, B., P. Berke, Ph. Bouillard, J. Vantomme, and T. J. Massart. 2011. "Investigation of the Influence of Design and Material Parameters in the Progressive Collapse Analysis of RC Structures." *Engineering Structures* 33(10):2805–20.

Sciegaj, Adam, Fredrik Larsson, Karin Lundgren, Filip Nilenius, and Kenneth Runesson. 2019. "A Multiscale Model for Reinforced Concrete with Macroscopic Variation of Reinforcement Slip." *Computational Mechanics* 63(2):139–58.

Shaikh, Faiz Uddin Ahmed. 2018. "Effect of Cracking on Corrosion of Steel in Concrete." *International Journal of Concrete Structures and Materials* 12(1):3.

Shiradhonkar, Saurabh R., and Ravi Sinha. 2018. "Maximum and Residual Flexural Crack Width Estimation in Reinforced Concrete Frame Members under Seismic Excitation." *Journal of Structural Engineering* 144(8):4018121.

Teng, Tso Liang, Yi An Chu, Fwu An Chang, and Hua Sheng Chin. 2004. "Simulation Model of Impact on Reinforced Concrete." *Cement and Concrete Research* 34(11):2067–77.

Unger, Jörg F., and Stefan Eckardt. 2011. "Multiscale Modeling of Concrete." *Archives of Computational Methods in Engineering* 18(3):341.

Voyiadjis, George Z., and Peter I. Kattan. 2017. "Mechanics of Damage, Healing, Damageability, and Integrity of Materials: A Conceptual Framework." *International Journal of Damage Mechanics* 26(1):50–103.

Wriggers, P., and S. O. Moftah. 2006. "Mesoscale Models for Concrete: Homogenisation and Damage Behaviour." *Finite Elements in Analysis and Design* 42(7):623–36.

Wu, T., and P. Wriggers. 2015. "Multiscale Diffusion–Thermal–Mechanical Cohesive Zone Model for Concrete." *Computational Mechanics* 55(5):999–1016.

Zou, Wennan, Qichang He, Mojia Huang, and Quanshui Zheng. 2010. "Eshelby's Problem of Non-Elliptical Inclusions." *Journal of the Mechanics and Physics of Solids* 58(3):346–72.

List of Figures

List of Tables